BOLETIN DE LA SOCIEDAD ESPAÑOLA DE
Cerámica y Vidrio
A R T I C U L O

Effect of Pb substitution on the thermoelectrical properties of textured $Bi_2Ca_2Co_{1.7}O_y$ ceramics prepared by a polymer solution method

SH. RASEKH[1], M.A. MADRE[1], J.C.DIEZ[1], E. GUILMEAU[2], S. MARINEL[2], A. SOTELO[1]

[1]ICMA (Universidad de Zaragoza-CSIC), Depto. de Ciencia y Tecnología de Materiales y Fluidos, C/María de Luna 3, E-50018, Zaragoza (Spain)
[2]CRISMAT Laboratory, UMR 6508 CNRS-ENSICAEN, 6 Bld. Maréchal Juin, 14050 Caen cedex (France)

Thermoelectrical properties of cobaltite ceramics can be tuned up by choosing the adequate synthetic method, cation substitution and subsequent grain orientation. This can be performed preparing the ceramics by a polymer solution method, using Pb partially substituting Bi, and texturing by directionally growing from the melt. In this work, $Bi_{2-x}Pb_xCa_2Co_{1.7}O_y$ (x = 0.0, 0.2, 0.4 and 0.6) ceramics, prepared by a polymer solution method, have been directionally grown, with the Laser Floating Zone (LFZ) technique, at 30 mm/h. In all the cases, the microstructure shows alternated layers with small CoO inclusions. It has been found a very important decrease on the resistivity and, at the same time, on the thermopower. However, the power factor values are improved with Pb addition, reaching power factor values, for samples with 0.4 Pb substitution, as high as two times the values obtained for undoped ones.

Keywords: Processing, Melting, Electrical properties, Thermopower, Misfit cobaltites.

Efecto de la sustitución del plomo sobre las propiedades termoeléctricas de cerámicos texturados $Bi_2Ca_2Co_{1.7}O_y$ obtenidos por el método de solución polimérico

Las propiedades termoeléctricas de cerámicas basadas en óxidos de cobalto pueden ser ajustadas eligiendo adecuadamente el método de síntesis, la substitución catiónica y posterior orientación de grano. Esto puede realizarse preparando las cerámicas precursoras por un método de solución con adición de un polímero, substituyendo parcialmente el Bi por Pb y texturando el material por crecimiento direccional a partir del fundido. En este trabajo, cerámicas con composición $Bi_{2-x}Pb_xCa_2Co_{1.7}O_y$ (x = 0.0, 0.2, 0.4 y 0.6), han sido preparadas por un método en disolución y crecidas direccionalmente con la técnica de Zona Fundida Flotante Inducida por láser (LFZ), a 30 mm/h. En todos los casos, la microestructura está formada por capas alternas con pequeñas inclusiones de CoO. Se ha encontrado una apreciable disminución en los valores de resistividad y, al mismo tiempo, del poder termoeléctrico .Sin embargo, el factor de potencia aumenta con la adición de plomo, llegando a doblar, en muestras con una adición del 0.4 Pb, los valores obtenidos para las muestras sin dopar.

Palabras clave: Procesamiento, Fusión, Propiedades eléctricas, Poder termoeléctrico, Cobaltitas.

1. INTRODUCTION

Nowadays thermoelectric (TE) materials are widely studied due to their ability for transforming the temperature gradient directly into an electric potential due to the well-known Seebeck effect. This phenomenon makes them promising materials for harvesting wasted energy, in form of heat, generated in different energy conversion systems (1).

The efficiency of the TE materials is characterized by a dimensionless factor known as figure of merit (2), $ZT = S^2T/\rho\kappa$, or by their power factor, $PF = S^2/\rho$, where T is the working temperature, S, Seebeck coefficient (or thermopower, TEP), ρ, electrical resistivity and κ, thermal conductivity.

Today, a wide range of alloys with high ZT values, such as Bi_2Te_3, have been industrially applied (3,4). This group of materials shows some drawbacks, as they can be degraded at high temperatures and/or releasing toxic elements. These problems lead to the limitation of their working temperature. This limitation was overwhelmed by the discovery in 1997 (5) of attractive thermoelectric properties in ceramics such as $Na_2Co_2O_4$. Thus, the CoO ceramic families attracted attention as promising thermoelectric materials for high temperature applications, leading to the discovery of new materials, such as $Ca_3Co_4O_9$, $Bi_2Sr_2Co_2O_9$ and $Bi_2Ca_2Co_2O_y$ with high thermoelectric properties (6-9).

Crystallographic studies on these materials have shown that they are formed by an alternate stacking of a common conductive CdI_2-type CoO_2 layer with a two-dimensional triangular lattice and a block layer composed of insulating rock-salt-type (RS) layers. The two sublattices (RS block and CdI_2-type CoO_2 layer) possess common a- and c-axis lattice parameters and β angles, but different b-axis length, causing a misfit along b-direction (10-12). Moreover, it has been found that the modification of the RS layer size changes the misfit relation of the two subsystems and, as a consequence, modifies the Seebeck factor (9). Some cation substitutions have shown to be adequate to change the RS layer size improving TEP when cation size is decreased, *e.g.* substitutions of Sr^{+2} for Ca^{+2} (13).

Another way allowing tuning up the TE properties is the aliovalent cationic substitution, *e.g.* La^{+3} for Ca^{+2} (14), which changes the electronic charge in the RS layer and, as a consequence, the relationship between Co^{+3} and Co^{+4} in the conductive layer. The changes on these proportions are responsible for the modifications on the TE properties (15), increasing the Co^{+3} proportion and, as a consequence, raising TEP values.

Taking the above considerations, Pb^{+2} substtitution for Bi^{+3} has demonstrated to be a successful route in order to improve the electrical resistivity and power factor in Bi-based cobaltites (16) even if TEP is decreasing.

On the other hand, the high structural anisotropy of this type of materials leads to the formation of plate-like grains during the crystallisation. This shape anisotropy opens the route to align preferentially the grains to obtain textured ceramics with thermoelectric properties, mainly on the electrical resistivity, comparable to those obtained for single crystals. Numerous methods have been reported to be useful to obtain a good grain alignment in ceramic materials, such as hot uniaxial pressing (17), spark plasma sintering (18), laser zone melting (LFZ) (19), templated grain growth (TGG) (20), *etc*.

The aim of this work is studying the effect of Pb addition on microstructure and TE properties of textured $Bi_2Ca_2Co_{1.7}O_y$, prepared by a polymer solution method developed in our laboratory (21,22), which has shown to be useful improving thermoelectrical performances of pure $Bi_2Ca_2Co_{1.7}O_y$ (23).

2. EXPERIMENTAL

Polycrystalline powders with nominal compositions $Bi_{2-x}Pb_xCa_2Co_{1.7}O_y$ (x = 0, 0.2, 0.4, 0.6) were prepared by a solution method from $Bi(CH_3CO_2)_3$ (99.99 + %, Aldrich), $Ca(CH_3CO_2)_2 \bullet 2H_2O$ (99%, Panreac), $Pb(CH_3CO_2)_2 \bullet 2H_2O$ (99%, Aldrich), and $Co(CH_3CO_2)_2 \bullet 4H_2O$ (98%, Panreac) commercial powders. They were weighed in the appropriate proportions and suspended in distilled H_2O. Glacial acetic acid (ACS Reagent, Panreac) was added dropwise to the above suspension until a pink clear solution was formed. Polyethylenimine (PEI) (50% aqueous, Aldrich) was then added and the solution turned darker immediately, due to the nitrogen-metal coordination. After partial evaporation of solvent (between 80 and 90 vol. %) in a rotary evaporator, the concentrated solution was placed onto a hot plate until a very dark pink thermoplastic paste is formed. Further heating turned this paste to violet colour, followed by a slow combustion with the release of brown fumes (nitrogen oxides). The resulting powder was milled and calcined at 750 and 800 ºC for *c.a.* 12 h, with an intermediate milling. This calcination process has been fixed in previous studies (24) to specifically decompose the alcaline earth carbonates avoiding their decomposition in the LFZ process, which would lead to bubble formation inside the melt, disturbing the crystallization front. The so obtained powders were then cold isostatically pressed at 200 MPa in order to obtain green cylindrical ceramic bars, which were subsequently used as feed in a LFZ device equipped with a continuous power Nd:YAG solid sate laser (1.06 μm) described elsewhere (25).

The growth conditions were optimized for all the compositions to obtain final cylindrical textured rods with high geometrical homogeneity. The growth process has been performed at 30 mm/h. On the other hand, the compositional homogeneity of the melt has been assured by the rotation of the seed at 3 rpm clockwise and 15 rpm anticlockwise for the feed. Therefore, rods with diameter from 2 to 3 mm and up to 30 cm length, depending on the precursor feed size, were obtained.

Characterization of the crystal structure has been performed by powder X-ray diffraction (XRD), at room temperature, with 2θ between 10 and 40 degrees, using a Siemens Kristalloflex diffractometer, working with Cu Kα radiation. Microstructure and phase distribution have been studied from micrographs recorded from longitudinal polished surfaces using a SEM (JEOL 6000) equipped with an energy dispersive spectroscopy (EDS) device. TE properties (electrical resistivity and thermopower) were determined simultaneously in a ZEM-3 system (ULVAC) at temperatures between 60 and 625 ºC.

3. RESULTS AND DISCUSION

Powder XRD diagrams of $Bi_{2-x}Pb_xCa_2Co_{1.7}O_y$ samples are presented in figure 1, which clearly shows that all the samples have similar patterns, independently of the Pb content. The peaks marked with an * correspond to the thermoelectric phase where the (002*l*) crystallographic planes are indicated, in agreement with the reported data for the $Bi_{2-x}Pb_xCa_2Co_2O_y$ structure (10). The peaks marked with a + are associated to the orthorhombic $Bi_6Ca_4O_{13}$ secondary phase (26) while the ▼ at 29.8 degrees indicates the peak corresponding to the (110) plane of the cubic $(Bi,Pb)_2Ca_2O_5$ secondary phase (27). The ■ indicates the (111) peak of Si used as reference. As it can be observed in figure 1a, for the Pb-free sample an additional peak at 21.65 degrees is appearing, corresponding to the orthorhombic BiCaO secondary phase. Pb addition clearly reduces the relative intensity of the diffraction peaks associated to the Bi(Pb)CaO secondary phase, indicating a reduction on the amount of this phase. Moreover, for samples with x = 0.6 Pb the peak at 29.4 degrees disappears while the one at 29.8 degrees raises, indicating the modification of the Bi(Pb)CaO crystalline structure from the orthorhombic to a cubic system. This effect can be related with the drastic change on the phase diagram induced by Pb (28).

Other effect of the Bi substitution by Pb, in the RS layer, is the raising of the cell parameters in the TE phase, displacing the XRD peaks towards lower angles. This effect is illustrated in figure 2, using the (0010) peak. From this peak, it has been calculated the evolution of the c-parameter as a function of Pb substitution, showing a linear behaviour, as can be clearly seen in the insert in figure 2. These results indicate that there is a linear relationship between the Pb addition tested in this work and the amount of Bi that can be substituted in the crystal structure when they are melt-processed.

The high texture obtained by the LFZ technique is illustrated by the SEM micrograph of a fractured surface shown in figure 3. As it can be observed, the textured samples are constituted by highly aligned microscopic grains which, in turn, are composed of many, well stacked and very thin, plate-like grains (~ 0.4 μm thickness) with a large surface area (more than 60 x 60 μm^2).

The micrographs shown in figure 4 correspond to polished longitudinal sections of the as grown samples, with

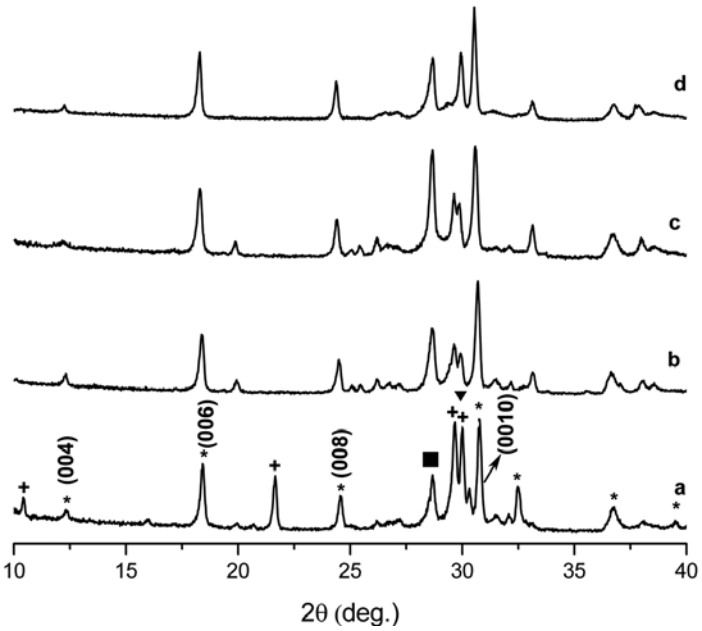

Fig. 1. Powder X-ray diffraction patterns obtained for the $Bi_{2-x}Pb_xCa_2Co_{1.7}O_y$ samples; x = 0 (a); 0.2 (b); 0.4 (c); and 0.6 (d). Thermoelectric phase peaks are indicated by an *, (002l) crystallographic planes are identified. Secondary orthorhombic Bi(Pb)CaO phase peaks are marked by an +, and secondary cubic Bi(Pb)CaO phase peak by an ▼. The ■ shows the Si (111) diffraction peak, used as reference.

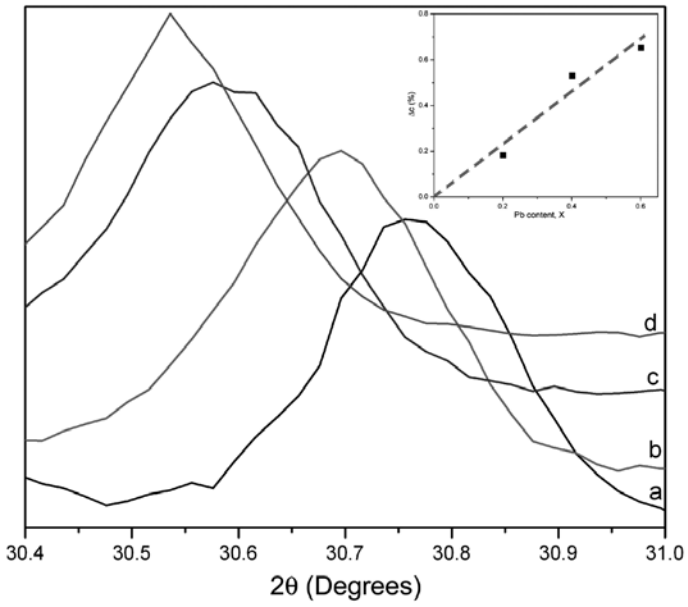

Fig. 2. Enlarged view of the (0010) diffraction peaks of $Bi_{2-x}Pb_xCa_2Co_{1.7}O_y$ samples for x = 0.0 (a); 0.2 (b); 0.4 (c); and 0.6 (d), showing their displacement as a function of Pb content. The insert illustrates the relative c-axis variation with respect to the undoped samples.

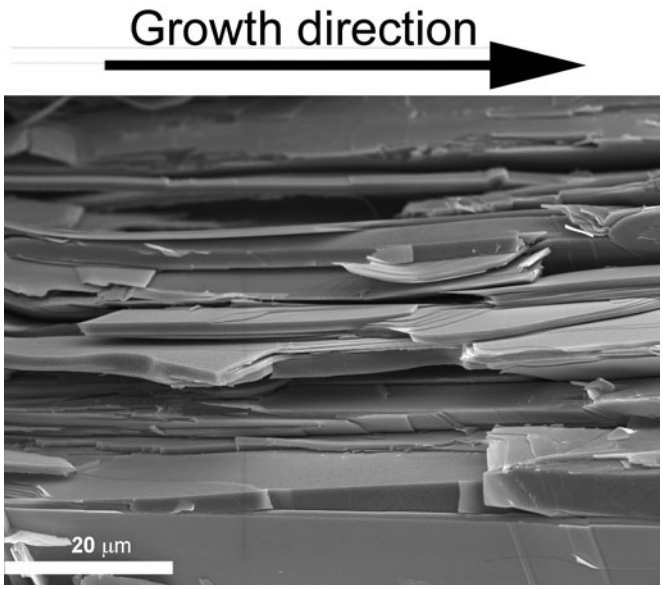

Fig. 3. SEM micrograph of a fractured $Bi_{2-x}Pb_xCa_2Co_{1.7}O_y$ sample, showing the alignment and stacking of the plate-like grains.

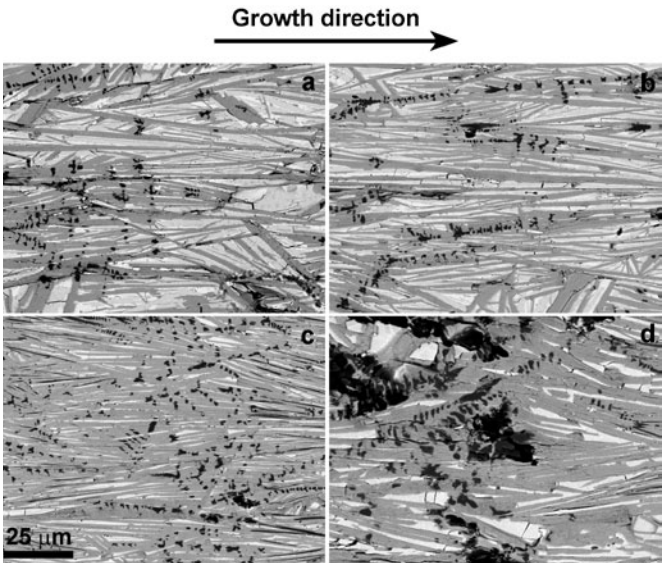

Fig. 4. SEM micrographs of longitudinal polished sections of the $Bi_{2-x}Pb_xCa_2Co_{1.7}O_y$ samples, for x = 0.0 (a); 0.2 (b); 0.4 (c); and 0.6 (d). The arrow indicates the growth direction.

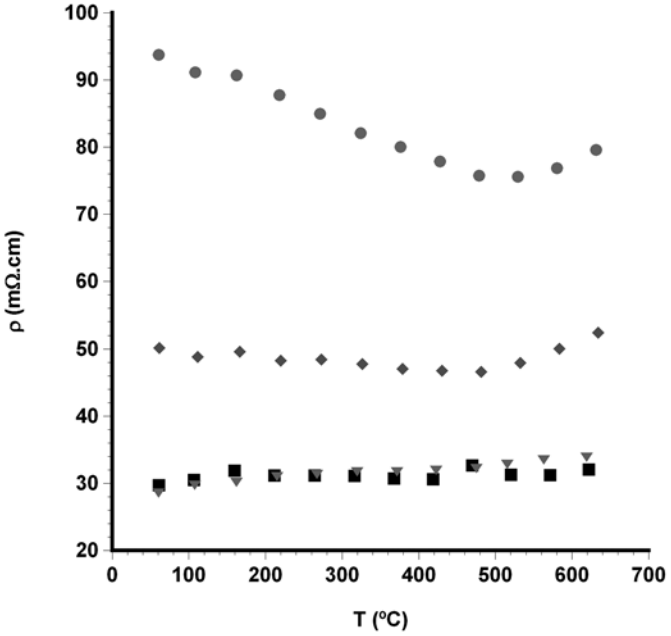

Fig. 5. Temperature dependence of the electrical resistivity, ρ, as a function of Pb content in $Bi_{2-x}Pb_xCa_2Co_{1.7}O_y$ samples, for x = 0.0 (●); 0.2 (◆); 0.4 (■); and 0.6 (▼).

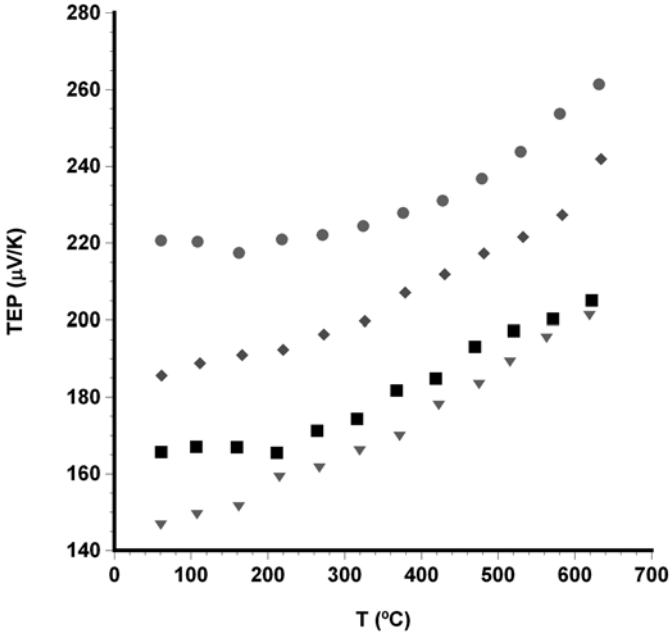

Fig. 6. Temperature dependence of the thermopower, or Seebeck coefficient, S, as a function of Pb content in $Bi_{2-x}Pb_xCa_2Co_{1.7}O_y$ samples, for x = 0.0 (●); 0.2 (◆); 0.4 (■); and 0.6 (▼).

TABLE I. ATOMIC % OF THE DIFFERENT ELEMENTS DETERMINED BY EDS FOR EACH CONTRAST OBSERVED BY SEM, AS A FUNCTION OF THE NOMINAL COMPOSITION.

Nominal composition	Contrast	Bi	Pb	Ca	Co
$Bi_2Ca_2Co_{1.7}O_y$	Dark grey	1.64(2)	-	2	1.72(1)
	Light grey	1.24(3)	-	1	-
	Grey dendritic	-	-	0.092(1)	1
$Bi_{1.8}Pb_{0.2}Ca_2Co_{1.7}O_y$	Dark grey	1.78(5)	0.19(2)	2	1.59(1)
	Light grey	1.51(4)	-	1	-
	Grey dendritic	-	-	0.098(1)	1
$Bi_{1.6}Pb_{0.4}Ca_2Co_{1.7}O_y$	Dark grey	1.48(2)	0.35(1)	2	1.73(2)
	Light grey	1.60(5)	0.19(7)	1	-
	Grey dendritic	-	-	0.098(3)	1
	Black plate-like	0.12(1)	0.074(2)	2	2.61(1)
$Bi_{1.4}Pb_{0.6}Ca_2Co_{1.7}O_y$	Dark grey	1.41(3)	0.45(1)	2	1.77(4)
	Light grey	1.41(4)	0.61(2)	1	-
	Grey dendritic	-	-	0.098(3)	1
	Black plate-like	0.17(1)	0.10(1)	2	2.49(3)
	Black spot	-	-	1	0.02(1)

These chemical compositions have been normalized on Ca except for the grey dendritic contrast where Co has been used.

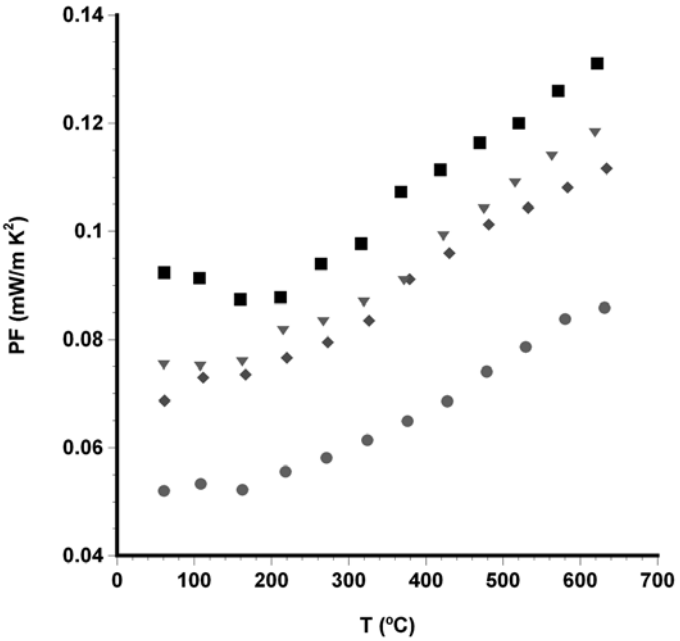

Fig. 7. Temperature dependence of the Power Factor, S^2/ρ, as a function of Pb content in $Bi_{2-x}Pb_xCa_2Co_{1.7}O_y$ samples, for x = 0.0 (●); 0.2 (◆); 0.4 (■); and 0.6 (▼).

different Pb substitution, where five different contrasts can be observed. EDS analysis (see Table I) allowed the compositional determination for each one. The dark grey contrast is associated to the misfit cobaltite phase, in agreement with the XRD data. Light grey phase is composed of bismuth and calcium oxides in a constant relationship Bi:Ca of 5:4 for Pb contents lower than 0.4. When Pb content increases, the cation relationship Bi(Pb):Ca of this phase changes to, approximately, 2:1 for a 0.4 content Pb and to 11:5 for samples with 0.6 Pb. The very dark grey contrast which can be seen as dendritic-like shape corresponds to CoO, with a very small amount of Ca. All the above contrasts are found in all the samples but for high Pb contents (x > 0.2 Pb) two more contrasts can be found (see figure 4c and d): black contrast with plate-like shape with a composition close to the thermoelectric Ca-349 phase, and small black spots identified as CaO appearing only in appreciable amounts in the 0.6 Pb substituted samples. On the other hand, clear differences can be observed in the microstructure, as a function of Pb content. Firstly, it is found a significant increase in the amount of the main thermoelectric phase from the undoped samples to the 0.4 Pb ones. Further Pb addition starts to decrease the proportion of thermoelectric phase. Secondly, the same evolution has been observed in the size and alignment of the thermoelectric phase grains. As a consequence of the variation on the thermoelectric phase content with Pb, a reduction of the impurities is produced until 0.4 Pb substitution. Further Pb addition starts to increase again the amount of the secondary phases.

This evolution could be explained using the phase diagram Bi-Pb-Ca-Co-O, still not determined, in our knowledge. In order to find a suitable explanation the ternary $BiO_{1.5}$-PbO-CaO phase diagram (28) has been revised. It has been found that increasing the Pb content a decrease on the melting point is produced. As a consequence, the growth process is drastically disturbed, as it can be clearly observed in figure 4d.

In figure 5 the evolution of the resistivity (ρ) with temperature (T), as a function of the Pb content, is represented for the as grown materials. Undoped samples show semiconductor behaviour from room temperature to about 550ºC and a metallic-like one for higher temperatures. For x = 0.2 Pb substituted samples a similar behaviour has been found. Moreover, for x > 0.2 Pb substituted samples the metallic-like behaviour is extended to all the measured temperature range, with very small dependence of resistivity with temperature. This can be explained by the substitution of Pb^{+2} for Bi^{+3}, which is promoting Co^{+3} to Co^{+4} and, as a consequence, increasing the carrier concentration due to the impurity compensation effect (29). However, the minimum resistivity values at room temperature have been obtained for heavily doped samples. For samples with x > 0.2 Pb substitution this value is about 30 mΩ.cm, which is, approximately, one third of the best ones reported in sintered specimens (10).

Figure 6, displays the variation of thermopower with temperature (T), as a function of the Pb content. S is positive in all cases which indicates a predominant hole conduction mechanism. It can also be observed a nearly linear increase of thermopower with temperature for all the samples, which is consistent with previously published data in layered cobaltites (30). The evolution of the thermopower with the Pb content is in agreement with the relationship between Co^{+3} and Co^{+4} in the CoO_2 layer, discussed above. The increase of carrier concentration due to the Pb incorporation in the structure is reflected in the reduction of the thermopower values. At near room temperature, S values decrease from, around, 220 μV/K obtained for the Pb-free samples, to around 145 μV/K for the 0.6 Pb one. These values are in agreement with the relationship between thermopower and Co^{+4} over the total amount of cobalt, determined by the Koshibae expression for a low spin state (15).

Evaluation of thermoelectric performances has been estimated using the power factor. Data for all the samples, as a function of temperature, are plotted in figure 7. Despite the negative influence of Pb on the thermopower, it can be clearly seen that Pb addition improves considerably the PF, compared with the undoped samples, due to the spectacular decrease on the electrical resistivity. When considering PF values at room temperature, they are ranging from around 0.050 mW/K².m, for the undoped samples, to a maximum of about 0.095 mW/K².m for the 0.4 Pb substituted sample.

4. CONCLUSIONS

This paper demonstrates that $Bi_{2-x}Pb_xCa_2Co_{1.7}O_y$ thermoelectric materials can be successfully directionally grown by the laser floating zone method (LFZ). This process leads to well textured samples with the Bi(Pb)-Ca-Co-O cobaltite phase as the major one. The texture is improved, and the amount of secondary phases is reduced, when increasing Pb substitution until x = 0.4. Further Pb addition leads to the degradation of the samples microstructure as well as the thermoelectrical properties.

In spite of the negative influence of Pb on the thermopower, a significative increase on the power factor has been obtained due to an important reduction obtained on the electrical resistivity. As a consequence, the power factor for the 0.4 Pb doped samples has reached values as high as, approximately, two times higher than the obtained for undoped samples.

5. ACKNOWLEDGEMENTS

The authors wish to thank the Gobierno de Aragón (Research Groups T12 and T74, and project PI154/08), the Spanish Ministry for Education and Science (Spanish-French Integrated Action HF2006-0171), and the Spanish Ministry of Science and Innovation (Project MAT2008-00429) for financial support. The technical contributions of C. Estepa, J. A. Gómez and C. Gallego are also acknowledged.

REFERENCES

1. G. Mahan, B. Sales, J. Sharp, Thermoelectric materials: New approaches to an old problem, Phys. Today, 50, 3, 42-47 (1997).
2. Thermoelectrics Handbook: Macro to Nano; D.M. Rowe, Ed.; CRC Press Taylor & Francis Group publications:Boca Raton, Fl. 2006; pp 1-3 to 1-7.
3. John Fairbanks, THERMOELECTRIC APPLICATIONS IN VEHICLES STATUS 2008, U.S. Department of Energy.
4. M.S. Bhatti, A Critical Look at R-744 and R-134a Mobile Air-Conditioning Systems, SAE Technical Paper, SAE-970527.
5. I. Terasaki, Y. Sasago, K. Uchinokura, Large thermoelectric power in $NaCo_2O_4$ single crystals, Phys. Rev. B, 56, 20, 12685-12687 (1997).
6. R. Funahashi, I. Matsubara, H. Ikuta, T. Takeuchi, U. Mizutani, S. Sodeoka, An oxide single crystal with high thermoelectric performance in air, Jpn. J. Appl. Phys., 39, 11B, L1127-L1129 (2000).
7. A. C. Masset, C. Michel, A. Maignan, M. Hervieu, O. Toulemonde, F. Studer, B. Raveau, J. Hejtmanek, Misfit-layered cobaltite with an anisotropic giant magnetoresistance $Ca_3Co_4O_9$, Phys. Rev. B, 62, 1, 166-175 (2000).
8. H. Leligny, D. Grebille, O. Perez, A. C. Masset, M. Hervieu, B. Raveau, A five-dimensional structural investigation of the misfit layer compound $[Bi_{0.87}SrO_2]_2[CoO_2]_{1.82}$, Acta Cryst. B, 56, Part 2, 173-182 (2000).
9. A. Maignan, D. Pelloquin, S. Hebert, Y. Klein, M. Hervieu, Thermoelectric Power In Misfit Cobaltites Ceramics: Optimization By Chemical Substitutions, Bol. Soc. Esp. Ceram. V., 45, 3, 122-125 (2006).
10. A. Maignan, S. Hébert, M. Hervieu, C. Michel, D. Pelloquin, D. Khomskii, Magnetoresistance and magnetothermopower properties of Bi/Ca/Co/O and Bi(Pb)/Ca/Co/O misfit layer cobaltites, J. Phys.: Condens. Matter., 15,17, 2711-2723 (2003).
11. H. Itahara, C. Xia, J. Sugiyama, T. Tani, Fabrication of textured thermoelectric layered cobaltites with various rock salt-type layers by using beta-$Co(OH)_2$ platelets as reactive templates, J. Mater. Chem., 14, 1, 61-66 (2004).
12. E. Guilmeau, M. Mikami, R. Funahashi, D. Chateigner, Synthesis and thermoelectric properties of $Bi_{2.5}Ca_{2.5}Co_2O_x$ layered cobaltites, J. Mater. Res., 20, 4, 1002-1008 (2005).
13. A. Maignan, S. Hébert, D. Pelloquin, C. Michel, J. Hejtmanek, Thermopower enhancement in misfit cobaltites, J. Appl. Phys. 92, 4, 1964-1967 (2002).
14. J. Nan, J. Wu, Y. Deng, C.-W. Nan, Thermoelectric properties of La-doped Ca–Co–O misfit cobaltites, Solid State Communications 124, 243-246 (2002).
15. W. Koshibae, K. Tsutsui, S. Maekawa, Thermopower in cobalt oxides, Phys. Rev. B., 62, 6869-6872 (2000).
16. T. Itoh, I. Terasaki, Thermoelectric properties of $Bi_{2.3-x}Pb_xSr_{2.6}Co_2O_y$ single crystals, Jpn. J. Appl. Phys. 39, 12A, 6658-6660 (2000).
17. V. Garnier, R. Caillard, A. Sotelo, G. Desgardin. Relationship among synthesis, microstructure and properties in sinter-forged Bi-2212 ceramics, Physica C, 319, 197-208 (19918. Yanfeng Zhang, Jiuxing Zhang, Qingmei Lu, Synthesis of highly textured $Ca_3Co_4O_9$ ceramics by spark plasma sintering, Ceram. International, 33, 1305-1308, (2007).
19. A. Sotelo, E. Guilmeau, M. A. Madre, S. Marinel, S. Lemonnier, J. C. Diez, $Bi_2Ca_2Co_{1.7}O_x$ thermoelectric ceramics textured by laser floating zone method,
Bol. Soc. Esp. Ceram. V., 47, 4, 225-228 (2008).
20. M. M. Seabaugh I. H. Kerscht, C. L. Messing, Texture development by templated grain growth in liquid-phase-sintered alpha-alumina J. Am. Ceram. Soc., 80, 5, 1181-1188 (1997).
21. G. F. de la Fuente, A. Sotelo, Y.Huang, M. T. Ruiz, A. Badia, L. A. Angurel, F. Lera, R. Navarro, C. Rillo, R. Ibañez, D. Beltran, F. Sapiña, A. Beltran, Polymer solution processing of (Bi,Pb)-Sr-Ca-Cu-O, Physica C, 185-189, 509-510 (1991).
22. A. Sotelo, H. Szillat, P. Majewski, F. Aldinger, Rapid synthesis of the Bi-2212 phase by a polymer matrix method, Supercond. Sci. Technol., 10, 717-720 (1997).
23. Sh. Rasekh, M. A. Madre, A. Sotelo, E. Guilmeau, S. Marinel, J. C. Diez, Effect of synthetic methods on the thermoelectrical properties of textured $Bi_2Ca_2Co_{1.7}O_x$ ceramics, Bol. Soc. Esp. Ceram. V. 49, 1, 89-94 (2010).
24. A. Sotelo, G. F. De la Fuente, F. Lera, D. Beltrán, F. Sapiña, R. Ibáñez, A. Beltrán, M. R. Bermejo, Novel polymer solution synthesis of the 110 K superconducting phase in the bismuth system, Chem. Mater., 5, 851-856 (1993).
25. G. F. de la Fuente, J. C. Diez, L. A. Angurel, J. I. Peña, A. Sotelo, R. Navarro, Wavelength dependance in laser floating zone processing. A case study with Bi-Sr-Ca-Cu-O superconductors. Adv. Mater., 7, 10, 853-856 (1995).
26. Standard ICSD card nº 01-080-1123.
27. Standard ICSD card nº 00-040-0314.
28. ACerS-NIST Phase Equilibria Diagrams CD-ROM Database v3.1, Fig. SII-447.
29. H. Q. Liu, Y. Song, S. N. Zhang, X. B. Zhao, F. P. Wang, Thermoelectrical properties of $Ca_{3-x}Y_xCo_4O_{9+\delta}$ ceramics, J. Phys. Chem. Solids, 70, 600-603 (2009).
30. T. Takeuchi, T. Kondo, T. Takami, H. Takahahsi, H. Ikuta, U. Mizutani, K. Soda, R. Funahashi, M. Shikano, M. Mikami, S. Tsuda, T. Yokoya, S. Shin, T. Muro, Contribution of electronic structure to the large thermoelectric power in layered cobalt oxides, Phys. Rev. B, 69, 125410 (2004).

Recibido: 20-11-2009
Aceptado: 5-7-2010